Arch. Mech., **66**, 6, pp. 411–428, Warszawa 2014

Normal contact stiffness of fractal rough surfaces

R. BUCZKOWSKI[1)], M. KLEIBER[2)], G. STARZYNSKI[2)]

[1)] *Division of Computer Methods*
Maritime University of Szczecin
Pobożnego 11, 70-507 Szczecin, Poland
e-mail: rbuczkowski@ps.pl

[2)] *Institute of Fundamental Technological Research*
Polish Academy of Sciences
Pawinskiego 5B, 02-106 Warsaw, Poland
e-mails: mkleiber@ippt.pan.pl,
gstarz@ippt.pan.pl

We used the fractal theory based on a single variable Weierstrass–Mandelbrot function to obtain the normal contact stiffness if rough and smooth isotropic surfaces are pressed against each other. Because in the original fractal theory the distribution of contact area is assumed geometrically, we propose the method in which the actual deformation of asperities and a correction due to asperity coupling (interaction) will be taken into account. This correction is equivalent to an increase of the effective separation by a quantity proportional to the nominal pressure and it has a significant effect on contact stiffness at larger normal loads (low separations). The numerical results demonstrate a nonlinear evolution of the contact stiffness with the normal load in particular in the first stage of loading at low squeezing pressures. We have compared the results of the theoretical contact stiffness using the fractal method with the experimental ultrasonic measurements. Experimental results made on real surfaces agree remarkably well with the theoretical predictions.

Key words: fractal model, contact stiffness, ultrasonic measurements.

Copyright © 2014 by IPPT PAN

1. Introduction

Measurement and prediction of both the normal and tangential stiffness has been studied in recent years by a number of authors [1–7]. Akarapu, Sharp and Robbins [3] point out that the contact area and normal stiffness rise linearly with the applied load. Medina, Nowell and Dini [4] propose a simple analytical model based on the classical work of Greenwood and Williamson and predict that the tangential stiffness is proportional to normal load and independent of the asperity radius and Young's modulus. Pohrt and Popov [5, 6] suggest a sublinear relationship between the normal stiffness and the nominal pressure.

They state that the power–law relationship observed for slowly apllied forces is valid for all apllied forces, with the exponent varying from 0.50 to 0.85, depending on fractal dimension. The results presented by Pohrt and Popov [5, 6] are not confirmed by Pastewka *et al.* [7] who have shown that the contact stiffness cannot be described by a power law for all apllied forces, and this would correspond to a straight line on log–log graph only. Several authors noted [2, 5, 8–11] that the expression for the microasperity contribution to the total elastic energy and the elastic stiffness depend on the elastic coupling between asperities. Some of them state that any derivation neglecting this interaction cannot describe the correct physics of realistic rough surfaces. Barber [10] has established an analogy between the electrical conduction and the contact stiffness in which the electrical conduction at any load is proportional to the elastic normal stiffness. This relation has been extended to the contact of finite bodies [11]. Measurements of the tangential contact stiffness between rough surfaces manufactured from titanium alloy using a digital image correlation method have been recently investigated by Kartal *et al.* [12].

In the paper we derive an expression for the normal contact stiffness (Sections 3 and 4) using the fractal theory (Section 2). The numerical results are compared with the experimental utrasonic measurements (Section 5). Last part contains the summary and conclusions.

2. Theoretical background

Fractal geometry, pioneered by Mandelbrot [13], can be observed in various natural phenomena. It is characterized by continuity, nondifferentiability and self-affinity. These mathematical properties are satisfied by the Weierstrass–Mandelbrot (WM) function given by [14–16]

$$z(x) = G^{(D-1)} \sum_{n=0}^{n_{max}} \frac{\cos(2\pi\gamma^n x)}{\gamma^{(2-D)n}}, \tag{2.1}$$

where $z(x)$ is the surface height, x is the lateral distance, D is the fractal dimension of a surface profile ($1 < D < 2$), γ is the scaling parameter for determining the spectral density and self–affine property ($\gamma > 1$). The right side of equation (2.1) is a superposition of cosine functions with geometrically increasing frequencies. The scaling parameter γ controls the density of the frequencies on the surface. Based on surface flatness and frequency distribution, γ is chosen to be 1.5 [14]. The fractal roughness G is a height scaling parameter independent of the frequency. A rougher surface is characterized by higher G values. The fractal dimension D determines the distribution of high- and low-frequency

with the surface profile components; larger values of D correspond to denser profiles. An effective way to obtain the fractal parameters is a structure function of order 2 [17]

$$S(\tau) = \frac{1}{L-\tau} \int_0^{L-\tau} [z(x) - z(x+\tau)]^2 \, dx. \tag{2.2}$$

In addition, the structure function is a function of the fractal parameters which can be expressed in the following form [17–19]:

$$S(\tau) = C\tau^{4-2D}, \tag{2.3}$$

τ is the displacement along x-direction and C is the scaling coefficient given by the formula

$$C = \frac{\Gamma(2D-3)\sin[(2D-3)\pi/2]}{(2-D)} G^{2(D-1)}. \tag{2.4}$$

For isotropic surfaces, the fractal parameter D can be obtained from the slope of the log–log plot of the structure function taken from equation (2.3)

$$\log S(\tau) = (4-2D)\log\tau + \log C. \tag{2.5}$$

In practise, the structure function $S(\tau)$ is determined in the following way. The profiles from a mesurement can be digitalized over a sampling length L. If the sampling spacing is Δt, with each sampling length L having $N+1$ evenly spaced data points [20],

$$z(x) = z_i, \qquad i = 0, 1, \ldots, N. \tag{2.6}$$

Assuming

$$\tau = n\Delta t, \qquad n = 1, 2, \ldots, \tag{2.7}$$

the discrete form of the structure function is

$$S(\tau) = S(n\Delta t) = \langle [z(x_i + n\Delta t)] - z(x_i)]^2 \rangle = \frac{1}{N-n} \sum_{i=0}^{N-n} (z_{i+n} - z_i)^2. \tag{2.8}$$

Hence, with the above relations both fractal parameters D and G can be calculated from the structure function (see Fig. 6).

3. Contact modelling

When two bodies with nominally flat surfaces are brought into contact, the area of real contact is only a small fraction of the nominal contact area where asperities from one solid are squeezed against asperities from another solid. The asperities can deform elastically or plastically.

Using a single term of the WM–function from equation (2.1) and assuming $n = 1$ we have

$$z(x) = G^{(D-1)} l^{(2-D)} \cos\left(\frac{2\pi x}{l}\right), \tag{3.1}$$

where l is the length scale (base diameter, Fig. 1) of an asperity at level n, such that $l_n = 1/\gamma^n$.

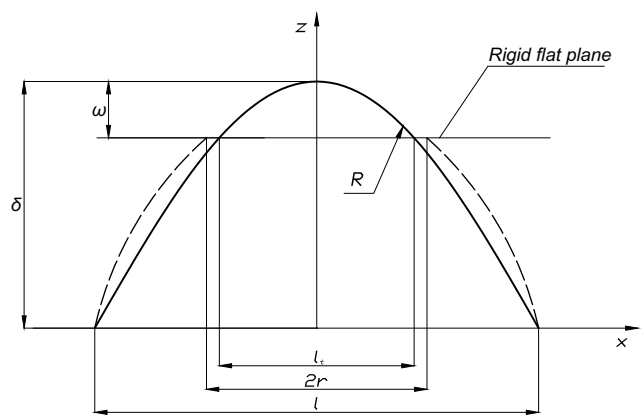

Fig. 1. Geometry of a contact spot. Here, l_t is a truncation diameter.

From equation (3.1), the asperity height δ equals

$$\delta = z(0) = G^{(D-1)} l^{(2-D)}, \tag{3.2}$$

and the radius of curvature at the asperity peak is then given

$$R = \frac{1}{|\partial z^2/\partial x^2|_{x=0}} = \frac{l^D}{4\pi^2 G^{(D-1)}}. \tag{3.3}$$

So, the approach ω is expressed as

$$\omega = \delta - z(\frac{l_t}{2}) = G^{(D-1)} l^{(2-D)} \left[1 - \cos\left(\pi \frac{l_t}{l}\right)\right] = G^{(D-1)} l^{(2-D)} q. \tag{3.4}$$

We now present a single contact model which is adopted from Majumdar and Bhushan [14], Yan and Komvopoulos [21], Jiang *at al.* [22] or Morag and

ETSION [23] and LIOU and LIN [24] models. Contrary to these models, which assume complete deformation of the asperity i.e. $\omega = \delta$ [21, 22], the present one suggests that the deformation of an individual asperity ω is an additional parameter independent of δ (but dependent on the acting loading) that can range from zero to complete deformation, i.e., $0 \leq \omega \leq \delta$ as it has been recently suggested by MORAG and ETSION [23].

The base diameter l is taken from equation (3.4)

$$l = \frac{\omega^{\frac{1}{2-D}}}{G^{\frac{D-1}{2-D}} q^{\frac{1}{2-D}}}. \tag{3.5}$$

After substituting l from equation (3.5), the radius of the curvature R from the expression (3.3) becomes

$$R = \frac{\omega^{\frac{D}{2-D}}}{4\pi^2 G^{\frac{2(D-1)}{2-D}} q^{\frac{D}{2-D}}}. \tag{3.6}$$

The contact load for an elastically deformed asperity (Hertz solution) is

$$W_e = \frac{4}{3} E R^{1/2} \omega^{3/2}. \tag{3.7}$$

Substituting R from equation (3.6) into equation (3.7) we obtain

$$W_e(\omega) = \frac{2}{3} E \frac{1}{\pi} \frac{1}{G^{\frac{D-1}{2-D}} q^{\frac{D}{2(2-D)}}} \omega^{\frac{3-D}{2-D}}. \tag{3.8}$$

The normal contact stiffness k_n at single asperity is defined as

$$k_n = \frac{\mathrm{d}W_e(\omega)}{\mathrm{d}\omega}. \tag{3.9}$$

From equations (3.8) and (3.9) we get

$$k_n = \frac{2}{3} E \frac{3-D}{2-D} \frac{1}{\pi} \frac{1}{G^{\frac{D-1}{2-D}} q^{\frac{D}{2(2-D)}}} \omega^{\frac{1}{2-D}}. \tag{3.10}$$

Following the Hertz theory, the contact area of the deformed asperity is given as

$$a = \pi R \omega \tag{3.11}$$

and with the help of equations (3.3), (3.4) and (3.5) it takes the form

$$a = \frac{1}{4\pi} l^2 q = \frac{1}{4\pi} q \frac{\omega^{\frac{2}{2-D}}}{G^{\frac{2(D-1)}{2-D}} q^{\frac{2}{2-D}}}. \tag{3.12}$$

Taking equations (3.10) and (3.11) into account we arrive at the following simple formula

$$k_n = \frac{4}{3\sqrt{\pi}} E \left(\frac{3-D}{2-D} \right) a^{1/2} \tag{3.13}$$

(similar equation has been recently given by Jiang *at al.* [22], but their line of reasoning is wrong.) Equation (3.13) can be rewritten as the function of ω (see Eq. (3.11))

$$k_n = \frac{4}{3} E \left(\frac{3-D}{2-D} \right) \sqrt{R\omega} \tag{3.14}$$

in which E denotes the effective Young's modulus given by

$$\frac{1}{E} = \frac{1-\nu_1^2}{E_1} + \frac{1-\nu_2^2}{E_2}, \tag{3.15}$$

where ν_1 and ν_2 are the Poisson's ratios and E_1 and E_2 are the Young's moduli of the two materials, respectively.

4. Contact stiffness

Greenwood [25] presented the random theory of surface roughness that we will briefly describe here.

Remark. The theory uses the central difference approximations in order to obtain the first and the second derivative for the slope and the curvature, respectively. So, in the case of non-differentiable Weierstrass–Mandelbrot function in which a grid or mesh of points and corresponding intervals are established this approximation technique is justified, and quantities like slope and curvatures are well-defined.

After introducing a standardized height z, slope m and curvature t

$$\zeta = z/\sigma, \qquad s = m/\sigma_2, \qquad t = -\kappa/\sigma_\kappa, \tag{4.1}$$

where σ, σ_2 and σ_κ are r.m.s. surface height (or standard deviation of the rough surface), r.m.s. slope and r.m.s. curvature, respectively, and assuming that $|s| < t\tan\theta$, the probability that an ordinate is a peak of height ζ and curvature t is

$$p(\zeta,t) = \frac{1}{(2\pi)^{3/2}\sqrt{(1-r^2)}} \exp\left(-\frac{1}{2} \frac{\zeta^2 + t^2 - 2r\zeta t}{1-r^2} \right) \times \int\limits_{-t\tan\theta}^{+t\tan\theta} \exp\left(-\frac{1}{2} s^2 \right) ds, \tag{4.2}$$

where $r = \sigma_m^2/\sigma\sigma_\kappa$ determines the character of the surface roughness, ${\sigma_m}^2 = \mathrm{E}[m^2]$, where $\mathrm{E}[m^2]$ denotes the element of the covariance matrix, here $\sigma_2 = \sigma_m \cos\theta$ and $\theta = \arcsin(h\sigma_\kappa/2\sigma_m)$. It is noted that $1 - r^2 = \cot^2(\theta)$. The variable r^{-2} corresponds to the Nayak's parameter $\alpha = m_0 m_4/m_2^2$ [26]. In the limit at sampling interval $h \to 0$ the quantities σ^2, σ_2^2 and σ_κ^2 become equal to the spectral moments of the profile m_0 (the zeroth), m_2 (the second) and m_4 (the fourth), respectively.

In the theory that follows we need probability density distributions of the peaks. To obtain these, Eq. (4.2) must be normalized by the ratio of peaks to ordinates N_p. The probability that an ordinate is a peak is found by integrating out the height and the curvature dependence, which according to GREENWOOD and WILLIAMSON [27] is equal in the closed form to

$$N_p = \int_{-\infty}^{+\infty} \int_{0}^{+\infty} p(\zeta, t) = \theta/\pi. \tag{4.3}$$

This formula can be taken as an ordinary check in the numerical evaluation of all improper integrals used here. The multiple integrals are evaluated using the Gauss–Legendre 50-point quadrature scheme.

By dividing Eq. (4.2) by N_p we obtain the second-order or joint probability density function $p_{peak}(\zeta, t)$ of the normalized heights ζ and curvatures $t = -\kappa/\sigma_\kappa$ of the peaks as

$$p_{peak}(\zeta, t) = \frac{1}{2\theta\sqrt{2\pi(1-r^2)}} \exp\left(-\frac{1}{2}\,\frac{\zeta^2 + t^2 - 2r\zeta t}{1-r^2}\right) \times \int_{-t\tan\theta}^{+t\tan\theta} \exp\left(-\frac{1}{2}s^2\right) ds. \tag{4.4}$$

Figure 2 presents the results of the numerical integration of the joint probability density function (Eq. (4.4)) with respect to the curvature to give the asperity height distribution. The asperity height distribution appears to be closely Gaussian with a skewness (the third moment normalized by the standard deviation σ) $Sk \neq 0$ and a kurtosis (the normalized fourth moment) $K \neq 3$. (The symmetric Gaussian distribution has the skewness $Sk = 0$ and the kurtosis $K = 3$.)

The total normal stiffness can be now determined by integrating the microstiffness k_n (see Eq. (3.14)) if the expected number of contact asperities is available. If there are N asperities (peaks) in all, the expected number of asperities $n(\eta)$ above given height $\zeta = z/\sigma$ for normalized separation $\eta = d/\sigma$

$$n(\eta) = N \int_{\eta}^{\infty} \int_{0}^{\infty} p_{peak}(\zeta, t)\, d\zeta\, dt. \tag{4.5}$$

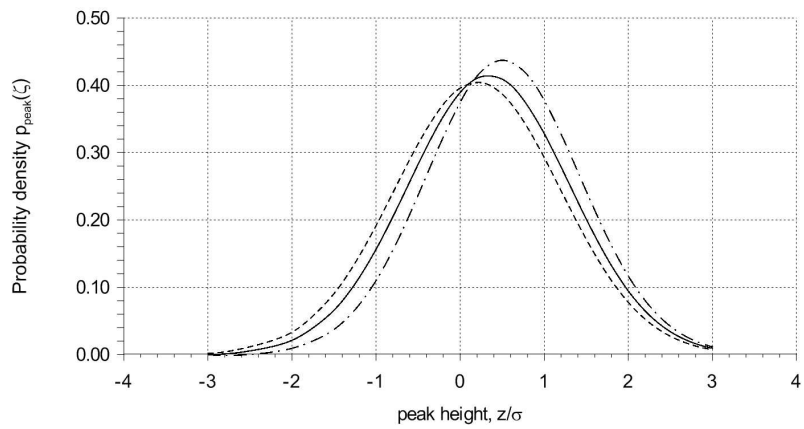

Fig. 2. The joint probability function of asperity height for varying r i $\theta = \pi/3$; r=1/2 (dot–dash), r=1/3 (solid line), r=1/5 (dashed line).

The results here were obtained for surface roughness which restricts θ to a range from $\theta = \pi/3$ to $\theta = \pi/4$ giving, from Eq. (4.3), such results that the number of peaks is always between 1/4 and 1/3 of the number of ordinates.

If the total number of peaks (the density of peaks D_p by the nominal area A_0 (see Table 1) is

$$N = A_0 D_p, \tag{4.6}$$

then the normal contact stiffness for all asperities becomes

$$K_n^e = \frac{4}{3} E\left(\frac{3-D}{2-D}\right) A_0 D_p \sigma^{1/2} \int_{\eta}^{\infty} \int_{0}^{\infty} \sqrt{R}(\zeta - \eta)^{1/2} p_{peak}(\zeta, t)\, d\zeta dt. \tag{4.7}$$

Because the radius R of the asperity peaks changes within the deformation process, the formula (4.7) is rewritten by replacing the radius of the peaks R by the inverse of the curvature, $R = 1/\kappa$, then (see description of Eq. (4.1))

$$R = \frac{1}{\sigma_\kappa t}, \tag{4.8}$$

where σ_κ denotes the standard deviation of the peak curvatures. So, the formula (4.7) is rewritten to be

$$K_n^e = \frac{4}{3} E\left(\frac{3-D}{2-D}\right) A_0 D_p \sigma^{1/2} \int_{\eta}^{\infty} \int_{0}^{\infty} \sqrt{1/(\sigma_\kappa t)}(\zeta - \eta)^{1/2} p_{peak}(\zeta, t)\, d\zeta\, dt. \tag{4.9}$$

We had no equipment to measure the standard deviation of the peak curvatures σ_κ. To obtain it, we used the formula given by Bush *et al.* [29]

$$\sigma_\kappa = \frac{3\sqrt{\pi}}{8R}. \tag{4.10}$$

The equivalent radius of asperities over all peak heights R has been measured and the values are given in Table 1.

It is known that the value of roughness parameters depend on the sampling interval used [30–33]. It is essential how they have been calculated. Indeed, we have not defined it directly, as the work aims at other issues. For clarity we describe a method of estimating these quantities that makes them independent of sampling interval. All surface topographies were measured with a scanning profilometer Hommel Tester T8000Nanoscan. The parameters were determined using the Hommel MapExpert program for surface (not profiles) measurements. The presented model requires height parameters describing a contact surface: R – mean radius of asperity and D_p – density of asperities. In the work [33] these relationships were carefully examined and a slight dependence of height parameters (R_a, R_q) on sampling interval was found, while the asperity radius and density heavily depend on sampling interval, which may yield completely different results from various measurements for the same surface. To avoid this, we have used our method, briefly described below, for the presented model to estimate magnitudes of the required parameters. The program Hommel Map has a function for determining 'islands' at any level of rough surface cross-section (Fig. 3). Starting from the maximum summit, the number of islands increases, and so does the calculated mean height of such islands.

We regard such an island as a cross-section of actual asperity and use the parameters mean height and mean surface (area) of island. Then we change such irregularity into a section of a paraboloid with a base area equal to the mean island surface area and height equal to the mean height of such an island. Thus we can calculate the radius of the summit of such solid asperity. A single area is a circle, equal to the mean area of a single island, representing a cross-section of a rotary paraboloid with radius of asperity R. Using these simple relations we can calculate the radius of asperity R based on the measured island surface. Cutting at various levels, we obtain a set of radiuses whose magnitude initially increases slowly, then for deeper cuts at approx. 30% levels radiuses increase rapidly. A similar procedure can be applied to estimate density D_p of contacting asperities (Fig. 4). This diagram below compares densities of asperities as a function of the bearing area (material ratio) for three examined surfaces. In the process of surface contact, the maximum density is a representative quantity. When the cutting level increases, the islands merge, the density of asperities

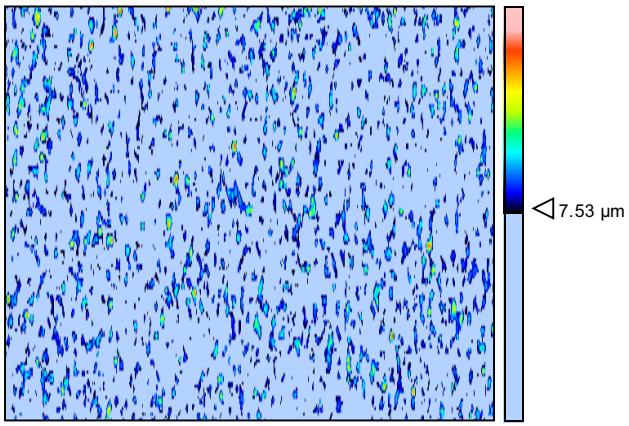

Number of islands	1180
Mean volume of islands	6439 µm3
Mean height of islands	6.64 µm
Mean surface of islands	0.00141 mm2
Mean height / surface ratio	4706 µm/mm2

Fig. 3. An example result of using the HommelMap function allowing to determine islands, their number and other parameters.

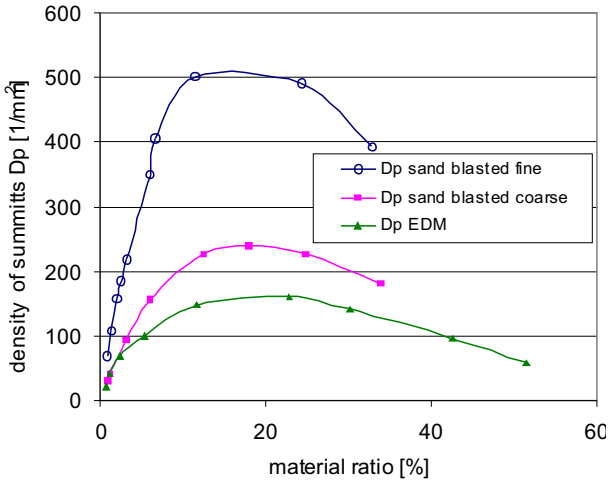

Fig. 4. Change in D_p – density of summits determined by the 'island' method as a function of bearing area (material ratio) for three examined surfaces.

reaches a maximum of about 20% of bearing area, and above it the density decreases and the radius increases rapidly. A representative summit radius can be determined for a bearing area corresponding to the determined density. We have

to bear in mind, however, that these considerations refer to islands, not summits calculated as per Greenwood's definition (point surrounded by points with lower coordinate z). The method is similar to that proposed by ARAMAKI (Aramaki–Majumdar–Bushan method [34, 35]), but it uses data from the entire examined surface of contact (surface area and height of islands), not matching paraboloids to profile fragments, as is the case in the cited work. The 'island' method is appropriate for describing the contact process because it neglects insignificant tiny summits that might appear in standard determination of parameters used by the Hommel Map program.

In the model, the effect of asperity interaction is taken into account. In equation (4.9) the correction is equivalent to an increase of the effective seperation by a quantity proportional to the nominal pressure as it has been suggested by CIAVARELLA, GREENWOOD and PAGGI [36]

$$\eta_{\text{new}} = \eta_{\text{old}} - \frac{W(\eta_{\text{old}})}{\sqrt{A_0}E\sigma}, \tag{4.11}$$

where A_0 is the nominal contact area which is equal here to $A_0 = 195\ \text{mm}^2$. We note that another method of asperitiy interaction based on finite or discrete element models has been recently proposed by MULVIHILL *et al.* [37], YASTREBOV *et al.* [38] and JERIER and MOLINARI [39].

5. Experimental set-up

The results of the theoretical contact model were compared to that measured experimentally. The experimental values of both the tangential and normal contact stiffness were determined from ultrasonic measurements by predictions of the reflection coefficient. The experiment was carried out using a set-up shown in Fig. 5. The stage enables precise measurement of the approach as a function of the contact pressure $W(\eta)/A_0$. The contact is realized between the flat rough surface of the upper specimen and the bottom special head having a very smooth surface ($R_a = 0.06$ μm). The specimens are made of carbon steel (0.45% carbon). The quasistatic load is applied gradually with a special device placed axially in a hydraulic press until a nominal pressure of 600 MPa is reached. The load is measured using a tensometric bridge and the resulting approach of the upper specimen is registered by a displacement (inductive) sensor. The results, in the form of diagrams of approach *vs.* contact pressure, are produced on-–line on a PC screen. The reflected ultrasonic signals are amplified by a defectoscope (flaw detector) and passed to the PC for further signal processing including spectral (frequency) analysis done by means of Fourier transform. The arrangement of the stage ensures uniform pressure distribution

in the contact zone using a precise auto—readjustment of a surface of tested specimen against a surface of a gauge head. The contact surface of the head (a counter specimen) is made in a form of three uniformly placed ring sectors (punches). Such arrangement increases accuracy by simultaneous measurement on each of three sectors. The counter specimen has two functions: a head for loading and an ultrasonic sender-receiver probe for acoustic waves in the shear (T) and longitudinal or normal (L) directions. Three piezoelectric transducers are used with different central frequency of 4 MHz and 7 MHz for the shear and longitudinal directions, respectively, to predict almost the same wavelengths in steel $\lambda = 0.8$ [mm]. For more details we refer the readers to the authors' paper [40].

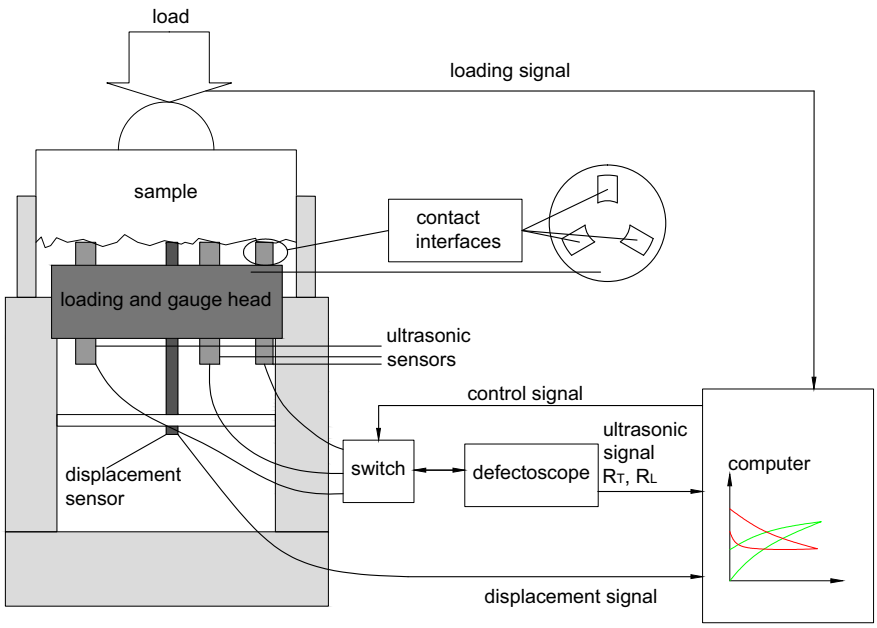

Fig. 5. Scheme of experimental set–up for simultaneous measurement of separation and reflection of ultrasonic waves R_T and R_L as a function of loading.

The idea of the measurement is simple. When asperity contact occurs, ultrasonic waves are transmitted across the interface and where an air gap exists between asperities (parts of the surfaces are out of contact), the waves are reflected back and the measured reflection coefficient is almost unity for all wave frequencies. It was demonstrated by others [41] that the reflection coefficient R_{12} at a partially contacting solid–solid interface is related to the contact stiffness per unit area of the interface by the following expression (if the two materials

on either side of the interface are identical):

$$R_{12} = \frac{1}{\sqrt{1 + \left(\frac{2K^e}{2\pi f z}\right)^2}}, \tag{5.1}$$

where $2\pi f$ is the angular frequency of the ultrasonic wave, z is the acoustic impedance (the product of the density of the material and the wave velocity through the material) and K^e denotes the stiffness (tangential or normal) per unit area of the interface. We note that similar methods of measurements of the contact stiffness based on ultrasonic apparatus have been recently described by KIM, BALTAZAR and ROKHLIN [42] and GONZALEZ–VALADEZ, BALTAZAR and DWYER–JOYCE [43].

6. Results and discussion

The surface roughness parameters including mechanical properties of the individual material and the fractal parameters are collected in Tables 1 and 2, respectively. The fractal parameters D and G are derived from the structure functions as was demonstrated in Section 1 (see Eqs. (2.2)–(2.8)). The plot of the structure function, for example machining process (sand blasted fine) is illustrated in Fig. 6.

Table 1. Surface roughness parameters for different machining processes ($E_1 = E_2 = 205000$ N/mm^2, $\nu_1 = \nu_2 = \nu = 0.3$, $Y = 400$ N/mm^2).

machining process	$\sigma = R_q$ [μm]	R [μm]	D_p [1/mm^2]	R_p [μm]
sand blasted (fine)	0.832	40	500	5.3
sand blasted (coarse)	5.13	30	230	15.3
electrical discharge machining	8.94	19	160	48

Table 2. Fractal parameters D and G for some machined surfaces.

machining process	D	G [m]
sand blasted (fine)	1.62	$1.2 \cdot 10^{-8}$
sand blasted (coarse)	1.58	$1.1 \cdot 10^{-7}$
electrical discharge machining	1.70	$8.2 \cdot 10^{-7}$

The results of the calculated (Eq. (4.9)) and experimental contact stiffness for different kind of machined processes are shown in Figs. 7–9. It can be concluded that the contact stiffness strongly depends on the machining method. Decreasing

the surface roughness increases the fractal dimension D which, in turn, increases the normal contact stiffness. In relation to the normal stiffness we conclude that the results based on fractal models and the experimental results are in close agreement but the statistical elastic models (the ones according to the work of Greenwood and Williamson [44]) always give poor results that are very much lower than the experimental ones. In calculations the effect of interactions between asperities has been taken into account [36]. This effect is dominant in the cases of smaller value of the standard deviation of the surface σ. The interaction effect increases considerably as the nominal pressure increases. On the other

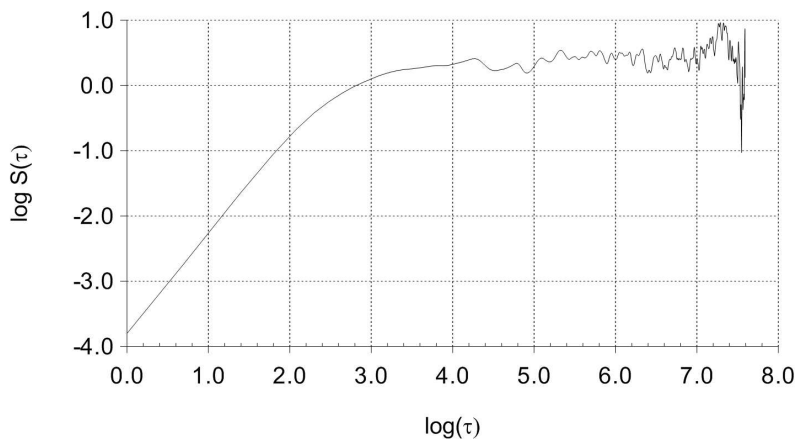

Fig. 6. Structure function of the profile (sand blasted fine).

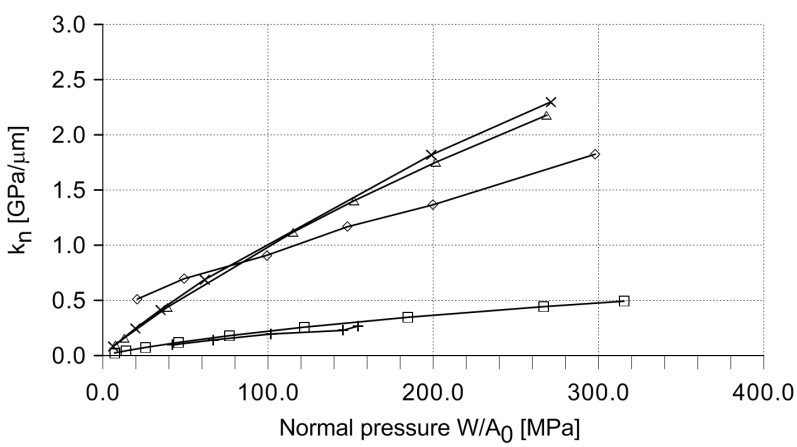

Fig. 7. Normal contact stiffness versus contact pressure (sand blasted fine). △ fractal model: $\theta = \pi/4$; × fractal model: $\theta = \pi/3$; □ statistical elastic model [28]; + based on [44]; ◇ experimental data.

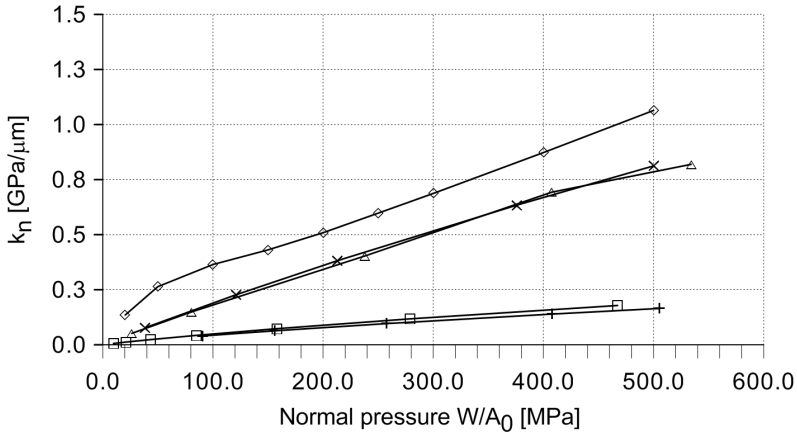

Fig. 8. Normal contact stiffness versus contact pressure (sand blasted coarse). △ fractal model: $\theta = \pi/4$; × fractal model: $\theta = \pi/3$; □ statistical elastic model [28]; + based on [44]; ◇ experimental data.

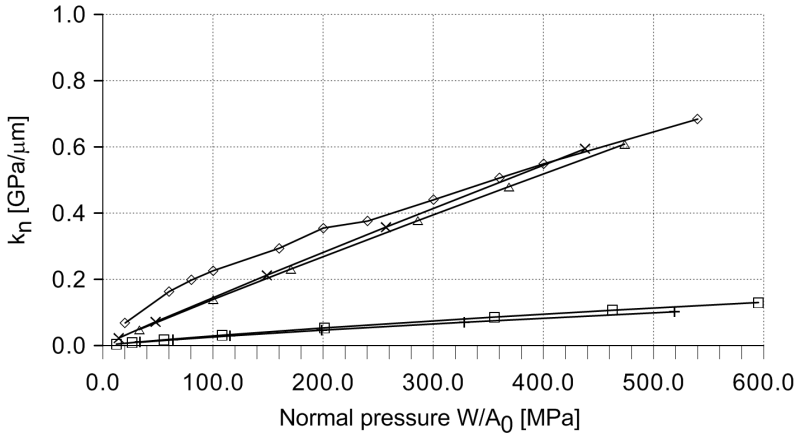

Fig. 9. Normal contact stiffness versus contact pressure (electrical discharge machining). △ fractal model: $\theta = \pi/4$; × fractal model: $\theta = \pi/3$; □ statistical elastic model [28]; + based on [44]; ◇ experimental data.

hand, for rough surfaces (sand blasted coarse and electrical discharge machining) the effect of the asperity interaction has practically no influence on the values of the contact stiffness.

For strongly anisotropic surfaces, with a grain pronounced to one direction the summits should be modelled by highly eccentric elliptic paraboloids rather than by caps. A more general dscription of such anisotropic surfaces has been recently presented by Buczkowski and Kleiber [45, 46].

7. Conclusions

1. The results based on the fractal model and the experimental ones are in close agreement. On the other hand, the results based on the statistical elastic models that have been obtained from [44] always give poor results that are very much lower than the experimental ones.

2. The contact stiffness is almost independent of the variable θ which determines the character of the surface roughness. As the variable θ varies, the contact stiffness changes slightly.

3. The corrected modification due to interaction between asperities has a significant effect on the contact stiffness for rough surfaces at higher normal loads. For low load levels, the interaction effect on the contact stiffness is minimal.

Acknowledgement

This study has been financed by the Ministry of Science and Higher Education under grant numbers N N519 402537 to the Maritime University of Szczecin, which is gratefully acknowledged.

References

1. M. Ciavarella, G. Murolo, G. Demelio, J.R. Barber, *Elastic contact stiffness and contact resistance for the Weierstrass profile*, J. of the Mechanics and Physics of Solids, **52**, 1247–1265, 2004.
2. C. Campañá, B.N.J. Persson, M.H. Müser, *Transverse and normal interfacial stiffness with randomly rough surfaces*, J. Phys.: Condens. Matter., **23**, 085001, 2011.
3. S. Akarapu, T. Sharp, M.O. Robbins, Stiffness of contact between rough surfaces, Physical Review Letters, **106**, 204301, 2011.
4. S. Medina, D. Nowell, D. Dini, *Analytical and numerical models for tangential stiffness of rough elastic contacts*, Tribology Lett., **49**, 103–115, 2013.
5. R. Pohrt, V.L. Popov, *Normal contact stiffness of elasic solids with fractal rough surfaces*, Physical Review Letters, **108**, 104301, 2012.
6. R. Pohrt, V.L. Popov, A.E. Filipov, *Normal contact stiffness of elasic solids with fractal rough surfaces for one- and three-dimensinal systems*, Physical Review, **E 86**, 026710, 2012.
7. L. Pastewka, N. Prodanov, B. Lorenz, M.H. Müser, M.O. Robbins, B.N.J. Persson, *Finite-size scaling in the interfacial stiffness of rough elastic contacts*, Physical Review, **E 87**, 062809, 2013.
8. C. Campañá, M.H. Müser, M.O. Robbins, *Elastic contact between self–affine surfaces: Comparison of numerical stress and contact correlation functions with analytical predictions*, J. Phys.: Condens. Matter., **20**, 354013, 2008.
9. M. Paggi, J.R. Barber, *Contact conductance of rough surfaces composed of modified RMD patches*, Int. J. of Heat and Mass Transfer, **54**, 4664–4672, 2011.

10. J.R. Barber, *Bounds on the electrical resistance between contacting elastic rough bodies*, Proc. R. Soc. Lond. A, **459**, 53–66, 2003.

11. J.R. Barber, *Incremental stiffness and electrical conductance in the contact of rough finite bodies*, Physical Review, **E 87**, 013203, 2013.

12. M.E. Kartal, D.M. Mulvihill, D. Nowell, D.A. Hills, *Measurements of pressure and area dependent tangential contact stiffness between rough surafces using digital image correlation*, Tribology Int., **44**, 1188–1198, 2011.

13. B.B. Mandelbrot, *Self-affine fractals and fractal dimension*, Physica Scripta, **32**, 257–260, 1985.

14. A. Majumdar, C.L. Tien, *Fractal characterization and simulation of rough surfaces*, Wear, **136**, 313–327, 1990.

15. A. Majumdar, B. Bhushan, *Role of fractal geometry in roughness characterization and contact mechanics of surfaces*, Trans. ASME, Journal of Tribology, **112**, 205–216, 1990.

16. S. Wang, K. Komvopoulos, *A fractal theory of the interfacial temperature distribution in the slow sliding regime: Part I. Elastic contact and heat transfer analysis*, Trans. ASME, Journal of Tribology, **116**, 812–823, 1994.

17. T.R. Thomas, B.-G. Rosen, N. Amini, *Fractal characterisation of the anisotropy of rough surfaces*, Wear, **232**, 41–50, 1999.

18. D.J. Whitehouse, *Handbook of Surface Metrology*, Institute of Physics Pub., Bristol and Philadelphia, 1994.

19. M.V. Berry, Z.V. Lewis, *On the Weierrstrass–Mandelbrot fractal function*, Proc. Roy. Soc. Lond., **A370**, 459–484, 1980.

20. L. He, J. Zhu, *The fractal character of processed metal surfaces*, Wear, **208**, 17–24, 1997.

21. W. Yan, K. Komvopoulos, *Contact analysis of elastic–plastic fractal surfaces*, Journal of Applied Physics, **84**, 3617–3624, 1998.

22. S. Jiang, Y. Zheng, H. Zhu, *A contact stiffness model of machined plane joint based on fractal theory*, Trans. ASME, Journal of Tribology, **132**, 011401-1-011401-7, 2010.

23. Y. Morag, I. Etsion, *Resolving the contradiction of asperities plastic to elastic mode transition in current contact models of fractal rough surfaces*, Wear, **262**, 624–629, 2007.

24. J.L. Liou, J.F. Lin, *A modifed fractal microcontact model developed for asperity heights with variable morphology parameters*, Wear, **268**, 133–144, 2010.

25. J.A. Greenwood, *A unified theory of roughness*, Proc. Roy. Soc. Lond., **A393**, 133–157, 1984.

26. P.B. Nayak, *Random process model of rough surfaces*, Trans. ASME, J. of Lubrication Technology, **93**, 398–407, 1971.

27. J.A. Greenwood, J.B.P. Williamson, *Developments in the theory of surface rughness*, in: Proc. 4th Leeds–Lyon Symp. on Tribology, D. Dowson *et al.* [Eds.], Mechanical Engineering Publications, London, 167–177, 1977.

28. R. Buczkowski, M. Kleiber, *A stochastic model of rough surfaces for finite element contact analysis*, Comput. Methods Appl. Mech. Engrg., **169**, 43–59, 1999.

29. A.W. Bush, R.D. Gibson, G.P. Keogh, *The limit of elastic deformation in the contact of rough surfaces*, Mech. Res. Comm., **3**, 169–174, 1976.

30. P. Pawlus, W. Zelasko, *The importance of sampling interval for rough contact mechanics*, Wear, **276–277**, 121–129, 2012.

31. M. Scaraggi, C. Putignano, G. Carbone, *Elastic contact of rough surfaces: A simple criterion to make 2D isotropic roughness equivalent to 1D one*, Wear, **297**, 811–817, 2013.

32. G. Zavarise, M. Borri-Brunetto, M. Paggi, *On the resolution dependence of micromechanical contact models*, Wear, **262**, 42–54, 2007.

33. S. Kucharski, G. Starzynski, *Study of contact of rough surfaces: Modeling and experiment*, Wear, **311**, 167–179, 2014.

34. A. Majumdar, B. Bhushan, *Fractal model of elastic-plastic contact between rough surfaces*, J. of Tribology ASME, **113**, 1–11, 1993.

35. H. Aramaki, H.S. Cheng, Y.W. Chung, *The contact between rough surfaces with longitudinal texture*, J. of Tribology ASME, **115**, 419–424, 1993.

36. M. Ciavarella, J.A. Greenwood, M. Paggi, *Inclusion of interaction in the Greenwood and Williamsson contact theory*, Wear, **265**, 729–734, 2008.

37. D.M. Mulvihill, M.E. Kartal, D. Nowell, D.A. Hills, *An elastic–plastic asperity interaction model for sliding friction*, Tribology Int., **44**, 1679–1694, 2011.

38. V.A. Yastrebov, J. Durand, H. Proudhon, G. Cailletaud, *Rough surface analysis be means of the Finite Element Method and of a new reduced model*, C.R. Mecanique, **339**, 473–490, 2011.

39. J.F. Jerier, J.F. Molinari, *Normal contact rough surfaces by the Discrete Element Method*, Tribology Int., **47**, 1–8, 2012.

40. G. Starzynski, R. Buczkowski, *Ultrasonic measurements of contact stiffness between rough surfaces*, J. of Tribology Trans. ASME **136**, No. 3, 034503–1, 2014.

41. B.W. Drinkwater, R.S. Dwyer–Joyce, P. Cawley, *A study of the interaction between ultrasound and a partially contacting solid–solid interface*, Proc. Roy. Soc. London, **A452**, 2613–2628, 1996.

42. J.-Y. Kim, A. Baltazar S.I. Rokhlin, *Ultrasonic assessement of rough surface contact between solids from elastoplastic loading–unloading hysteresis cycle*, J. of the Mechanics and Physics of Solids, **52**, 1911–1934, 2004.

43. M. Gonzalez–Valadez, A. Baltazar, R.S. Dwyer–Joyce, *Study of interfacial stiffness ratio of a rough surface in contact using a spring model*, Wear, **268**, 373–379, 2010.

44. J.A. Greenwood, J.B.P. Williamson, *Contact of nominally flat surfaces*, Proc. Roy. Soc. Lond., **A295**, 300–319, 1966.

45. R. Buczkowski, M. Kleiber, *Elasto–plastic statistical model of strongly anisotropic rough surfaces for finite element 3D-contact analysis*, Comput. Methods Appl. Mech. Engrg., **195**, 5141–5161, 2006.

46. R. Buczkowski, M. Kleiber, *Statistical models of rough surfaces for finite element 3D-contact analysis*, Arch. Comput. Methods Eng., **16**, 399–424, 2009.

Received January 2, 2014; revised version May 20, 2014.